Natural convection between two horizontal cylinders inside a circular enclosure subjected to external convection

C. J. Ho, Y. T. Cheng and C. C. Wang*
Department of Mechanical Engineering, National Cheng Kung University, Taiwan, Republic of China

This paper presents a numerical study, supplemented with experiments of flow visualization and holographic interferometric measurement, concerning the buoyancy-induced fluid flow and heat transfer between two horizontal, differentially heated cylinders inside a circular, air-filled enclosure subjected to external convection. Numerical simulations via a finite-difference method have been conducted mainly to investigate the effect of insulation (namely, the external convection boundary condition) at the circular enclosure wall on the buoyant air flow structure and heat transfer characteristics among the horizontal cylinders and the circular enclosure wall. The results are displayed graphically to emphasize the effects of the Rayleigh number ($Ra = 10^4 \sim 10^7$), the inclination angle of the enclosure with respect to gravity ($\phi_g = 30, 60, 90°$) and the gap width between the horizontal cylinders ($s/d = 0.7, 0.8333, 1.0$) in the presence of external convection. The external convection at the circular enclosure wall was found to further promote buoyant convection flow and a markedly enhanced heat transfer between the cylinders accordingly results. In addition, the simulation taking account for the external convection at the enclosure wall was found to compare favorably with the experimental results of flow visualization and temperature distribution in a test cell with imperfect thermal insulation.

Keywords: natural convection; enclosure flows

Introduction

In the present study, we examine the buoyancy-driven fluid flow and heat transfer between two horizontal, differentially heated cylinders inside a circular, air-filled enclosure subjected to external convective heat exchange with the ambient at a temperature $T_\infty(= T_m)$, as schematically depicted in Figure 1. This configuration is fundamentally relevant to heat tracing systems that are widely employed to actively balance heat loss of the piping system to the ambient, in order to prevent fluid inside the pipelines from condensing/freezing or becoming too viscous (Kohli 1979, Sandberg 1989). In an external tracing system, the pipeline (simulated as a cold cylinder) is heated to a specified temperature by placing a steam- or electricity-heated pipe (simulated as a hot cylinder) around the pipeline. The present paper is the result of a follow-up study to an earlier paper (Ho et al. 1993), in which details of the buoyant fluid flow and heat transfer in the same geometrical configuration as shown in Figure 1 (but with an adiabatic condition at the enclosure wall) were investigated. It should be noted that selection of the ambient temperature equal to the mean temperature of the hot and cold cylinder inside the enclosure is mainly to preserve a symmetry possessed by the resulting mathematical formulation of the problem, as shown in the earlier paper (Ho et al. 1993). From the flow visualization results of that work, it was found that heat exchange of air inside the enclosure with the ambient, due to the practical difficulty in achieving an adiabatic condition at the enclosure wall in the experiment, could exert a significant influence on the buoyancy-induced flow structure. Furthermore, the condition at the enclosure wall, in practice, can be approximated more realistically with the help of a convective boundary condition. The primary objective of the present study is, therefore, to investigate via a finite-difference simulation the effect of convection at the enclosure wall on the buoyant-convection heat transfer and fluid flow arising between the two cylinders inside the enclosure. Moreover, the present numerical prediction was compared with the experimental results of flow visualization and temperature distribution mapped in the test cell constructed in the earlier work (Ho et al. 1993). A holographic interferometry system (Ho and Lin 1991) was employed to visualize the natural-convection temperature field of air confined in the enclosure. The error in the experimental data of the Rayleigh number based on the uncertainty analysis (Kline and McClintock 1953) was found to be 2.3 percent.

As cited in the previous paper (Ho et al. 1993), very few studies have been devoted to the problem of buoyant-

*Present address: San-Fu Motor Corp., Taichung, Taiwan, Republic of China.

Address reprint requests to Professor Ho at the Department of Mechanical Engineering, National Cheng Kung University, Tainan, Taiwan 70101, Republic of China.

Received 9 December 1993; accepted 7 March 1994

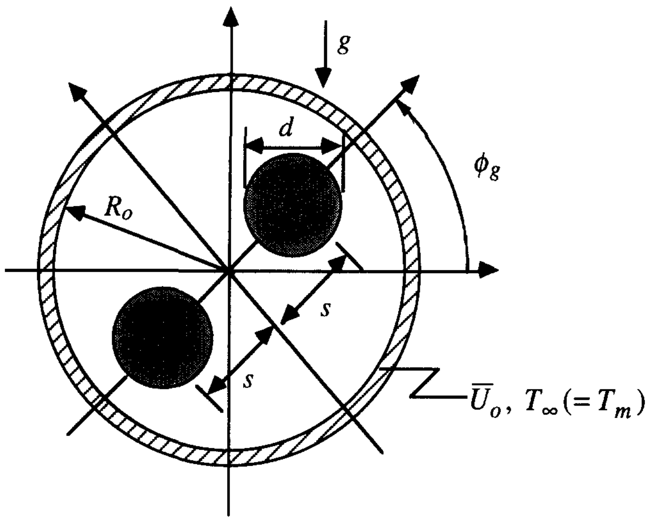

Figure 1 Schematic diagram of the physical configuration under consideration

convection heat transfer between heating elements in an enclosure. A series of experiments (Crupper and Warrington 1981, Warrington and Weaver 1990) has been reported for buoyancy-driven heat transfer from an array of horizontal cylinders to a cooled enclosure. Lacroix (1992) analyzed, by means of a finite-difference method, buoyant-convection heat transfer from two vertically separated cylinders to a rectangular enclosure cooled at the top.

Mathematical formulation and numerical method

The mathematical formulation for the steady, two-dimensional laminar, buoyancy-driven convection heat transfer inside the physical configuration illustrated in Figure 1 follows that described in the previous paper (Ho et al. 1993). Thus, there is no need to repeat that discussion here. In short, the fluid (air) inside the enclosure is modeled as Newtonian adhering to the Oberbeck-Boussinesq approximation. Viscous dissipation and compressibility effects are assumed to be negligible. The dimensionless, governing differential equations for the conservation of mass, momentum and energy are cast in terms of vorticity, stream function and temperature. In order to effectively deal with the geometrically complicated solution domain of the present problem, a composite overlapping mesh system is employed here so as to embed a general, curvilinear coordinate system for the interior among three cylindrical meshes around the circular solid boundaries—namely, surfaces of the two horizontal cylinders and the circular enclosure. On the basis of such a composite mesh system, the dimensionless, governing differential equations are written in cylindrical polar coordinates and general curvilinear coordinates, respectively. In the cylinder polar coordinates

$$\frac{1}{r}\frac{\partial\psi}{\partial\phi}\frac{\partial\omega}{\partial r}-\frac{1}{r}\frac{\partial\psi}{\partial r}\frac{\partial\omega}{\partial\phi}=\Pr\left[\mathrm{Ra}\left(\cos\phi\frac{\partial\theta}{\partial r}-\frac{\sin\phi}{r}\frac{\partial\theta}{\partial\phi}\right)+\nabla^2\omega\right] \tag{1}$$

$$\nabla^2\psi=-\omega \tag{2}$$

$$\frac{1}{r}\frac{\partial\Psi}{\partial\phi}\frac{\partial\theta}{\partial r}-\frac{1}{r}\frac{\partial\psi}{\partial r}\frac{\partial\theta}{\partial\phi}=\nabla^2\theta \tag{3}$$

where

$$\nabla^2\equiv\frac{\partial^2}{\partial r^2}+\frac{1}{r}\frac{\partial}{\partial r}+\frac{1}{r^2}\frac{\partial^2}{\partial\phi^2}$$

And in the curvilinear coordinates (Thompson et al. 1974),

$$\frac{1}{J}\left(U\frac{\partial\omega}{\partial\xi}+V\frac{\partial\omega}{\partial\eta}\right)=\Pr\left\{\frac{\mathrm{Ra}}{J}\left[\cos\phi_g\left(\frac{\partial y}{\partial\eta}\frac{\partial\theta}{\partial\xi}-\frac{\partial y}{\partial\xi}\frac{\partial\theta}{\partial\eta}\right)-\sin\phi_g\left(\frac{\partial x}{\partial\xi}\frac{\partial\theta}{\partial\eta}-\frac{\partial x}{\partial\eta}\frac{\partial\theta}{\partial\xi}\right)\right]+\tilde{\nabla}^2\omega\right\} \tag{4}$$

$$\tilde{\nabla}^2\psi=-\omega \tag{5}$$

$$\frac{1}{J}\left(U\frac{\partial\theta}{\partial\xi}+V\frac{\partial\theta}{\partial\eta}\right)=\tilde{\nabla}^2\theta \tag{6}$$

Notation

a_1, a_2, a_3	Geometric coefficients
Bi	Biot number, $(\bar{U}_o d/k)$
c	Specific heat
d	Diameter of cylinder
g	Gravitational acceleration
h	Heat transfer coefficient
J	Jacobian
k	Thermal conductivity
Nu	Nusselt number (Equation 10)
P	Coordinate control function
Pr	Prandtl number (ν/α)
Q	Coordinate control function
r^+	Radial coordinate
r	Dimensionless radial coordinate (r^+/d)
Ra	Rayleigh number $(g\beta[T_h - T_c]d^3/[\nu\alpha])$
R_i	Radius of cylinder $(d/2)$
R_o	Radius of circular enclosure
s	Half center spacing between cylinders
T	Temperature
T_m	Mean temperature $([T_h + T_c]/2)$
$\bar{U}_o$	Overall heat transfer coefficient
U, V	Contravariant velocity components

Greek symbols

α	Thermal diffusivity $(k/\rho c)$
β	Thermal expansion coefficient
η	Transformed coordinate
θ	Dimensionless temperature $([T - T_m]/[T_h - T_c])$
ν	Kinematic viscosity
ρ	Density
ξ	Transformed coordinate
ϕ	Angular coordinate
Φ	Angular location on cylinder surface
ϕ_g	Inclination angle
Ψ	Dimensionless stream function
ω	Dimensionless vorticity

Subscripts

c	Cold cylinder
h	Hot cylinder
m	Mean value
o	Circular enclosure
∞	Ambient fluid

where U and V are the contravariant velocity components along the ξ and η directions, defined as

$$U = \frac{\partial \psi}{\partial \eta}; \; V = -\frac{\partial \psi}{\partial \xi} \tag{7}$$

and

$$\tilde{\nabla}^2 \equiv \frac{1}{J^2}\left(a_1 \frac{\partial^2}{\partial \xi^2} - 2a_2 \frac{\partial^2}{\partial \xi \partial \eta} + a_3 \frac{\partial^2}{\partial \eta^2}\right) + P\frac{\partial}{\partial \xi} + Q\frac{\partial}{\partial \eta} \tag{8a}$$

$$a_1 \equiv \left(\frac{\partial x}{\partial \eta}\right)^2 + \left(\frac{\partial y}{\partial \eta}\right)^2 \tag{8b}$$

$$a_2 \equiv \frac{\partial x}{\partial \xi}\frac{\partial x}{\partial \eta} + \frac{\partial y}{\partial \xi}\frac{\partial y}{\partial \eta} \tag{8c}$$

$$a_3 \equiv \left(\frac{\partial x}{\partial \xi}\right)^2 + \left(\frac{\partial y}{\partial \xi}\right)^2 \tag{8d}$$

In Equation 8a, the coordinate control functions P and Q are based on the forms devised by Thomas and Middlecoff (1980).

The dimensionless boundary conditions of the problem considered are

$$\frac{\partial \psi}{\partial r} = \frac{\partial \psi}{\partial \phi} = 0, \; \psi = \psi_h(\text{constant}), \; \theta = 0.5 \tag{9a}$$

$$\frac{\partial \psi}{\partial r} = \frac{\partial \psi}{\partial \phi} = 0, \; \psi = \psi_c(\text{constant}), \; \theta = -0.5 \tag{9b}$$

on the surfaces of the two isothermally heated cylinders, respectively, and

$$\psi = 0, \; \frac{\partial \theta}{\partial r} + Bi\theta = 0 \tag{9c}$$

at the enclosure wall for which the external heat exchange with the ambient is modeled by an overall heat transfer coefficient $\bar{U}_o$, leading to a dimensionless parameter Biot number Bi.

The finite-difference method employed to solve the set of governing differential equations (Equations 1–6) subjected to the boundary conditions (Equation 9) is described in detail in (Ho et al. 1993) and obviates further elaboration here. In the iterative calculation procedure for the steady-state solution to the present problem, the unknown boundary stream functions on the two cylinders were updated based on the requirement of single-valuedness of pressure, which leads to evaluation of a line integral in terms of the newly obtained vorticity and temperature fields (Adlam 1986). The iterative calculation was carried out until a prescribed relative convergence criterion of 10^{-5} was satisfied for all the field variables of the problem. Moreover, an overall energy balance for the enclosure within 0.1 percent was achieved for all the converged calculations obtained.

On the basis of a series of mesh-sized independence tests for each submesh domain, three composite mesh systems were employed for the present calculations: [15 (radial) × 41 (angular), 5 (radial) × 89 (angular), 45 × 57 (curvilinear)], [15 × 41, 5 × 89, 45 × 55], [15 × 41, 5 × 101, 51 × 55] for $s/d = 0.7$, 0.8333 and 1.0, respectively. The first two submesh systems shown in the brackets are, the cylindrical meshes around surfaces of the cylinders and the circular enclosure wall respectively. The third submesh system is the curvilinear mesh for the interior region amid the solid circular boundaries.

Results and discussion

Simulations have been undertaken for the steady-state, buoyancy-driven fluid flow and heat transfer of air (Pr = 0.71) arising between the differentially heated cylinders inside a circular enclosure of $R_o/R_i = 4$, with the relevant dimensionless parameters in the following ranges: Ra = 10^4–10^7; s/d (center-to-center spacing between cylinders) = 0.7, 0.8333 and 1.0; ϕ_g (inclination angle of the enclosure) = 30°, 60° and 90°; and Bi = 0, 0.5 and 1.0.

Figure 2 illustrates the influence of the external convection at the enclosure wall, namely the Biot number Bi, on the flow structure (left) and temperature distribution (right) developed inside the circular enclosure at three orientation angles with Ra = 14,635 and $s/d = 0.8333$. The capital letters H and C centered at two cylinders in the contour plots of streamlines and isotherms shown in Figure 2 are used to indicate the hot and cold cylinder, respectively. For the vertical orientation, $\phi_g = 90°$, the symmetric flow structure with respect to both vertical and horizontal axes of the enclosure appears to be rather unaffected by the presence of external convection at the enclosure wall. But, the recirculating flow strength is greatly enhanced as indicated by the greater magnitude of the stream-function extreme for $Bi = 1.0$ shown in Figure 2. Meanwhile, the isotherms for the vertically oriented enclosure clearly reveal that the external heat change at the enclosure wall tends to induce further development of a thermal boundary layer around the horizontal cylinders, thus enhancing their heat transfer rates. Within the inclined enclosures, $\phi_g = 30°$ or 60°, as demonstrated in Figure 2, the influence of external convection is primarily on the structure of the counterclockwise recirculating flow channeling through the gap between the two cylinders. The split vortex structure for $Bi = 1.0$ can be seen to become further distinctive and strengthened in comparison to that for the adiabatic enclosure wall ($Bi = 0$). Furthermore, as compared to the flow visualization photograph obtained for $\phi_g = 60°$, Ra = 14,635 and $s/d = 0.8333$ displayed in Figure 3, a good agreement of the flow structure can be readily observed between the corresponding prediction (shown in Figure 2), accounting for the external convection $Bi = 1.0$ and the experiment. Moreover, thermal plume activity originating from hot or cold cylinder can be readily detected to intensify greatly as a result of the external heat exchange with the ambient through the enclosure wall.

In Figure 4, the streamline pattern and isotherm distribution under the influence of external convection of $Bi = 0.5$ at a different Rayleigh number is shown for $s/d = 0.7$ and $\phi_g = 30°$. As can be expected, the buoyant flow field inside the inclined enclosure is greatly strengthened with the increase of Ra. From the isotherm plots in Figure 4, it can be further noticed that with the increase of Ra, the thermal plume from the hot/cold cylinder tends to slant away from the adjacent cold/hot cylinder. Accordingly, the counterclockwise recirculating flow enclosing the two cylinders is increasingly expanded and reinforced with the increase of Ra. Moreover the temperature field becomes further stratified with the intensified buoyant flow resulting from the increase of Ra and a rather isothermal region arises above the hot cylinder and below the cold cylinder.

Figure 5, supplemented with the flow and temperature fields displayed in Figure 4, is intended to show the effect of the gap width between the two cylinders, s/d, on the buoyant fluid flow and temperature fields under the influence of external convection. Resembling that observed for the adiabatic enclosure (Ho et al. 1993), the recirculating flow field inside the enclosure subjected to external convection is found to be markedly impeded with the enlargement of the gap width, as

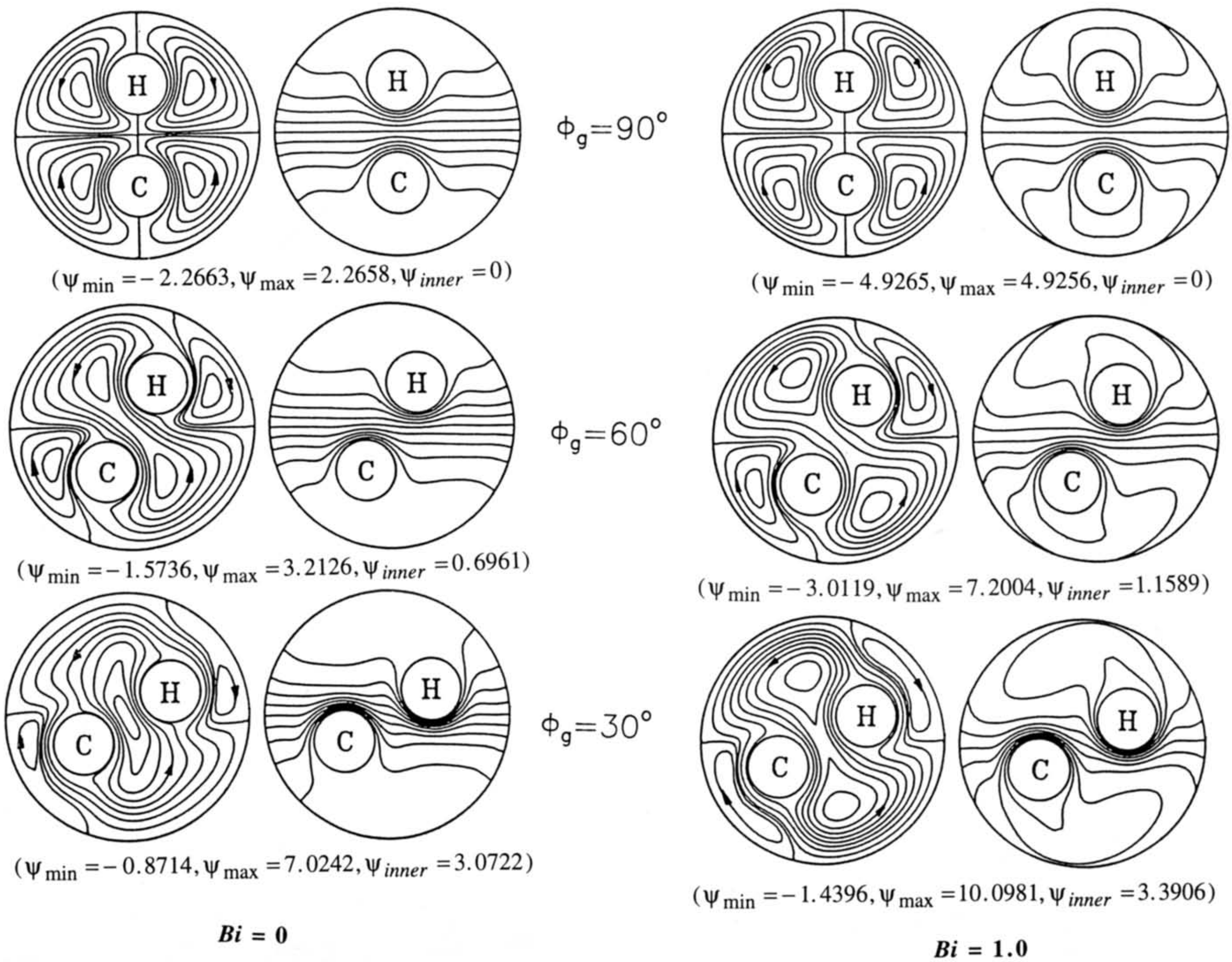

Figure 2 Influence of *Bi* on streamlines (left) and isotherms (right) for different orientation angle with $s/d = 0.8333$, Ra = 14,635 in a circular enclosure of $R_o/R_i = 4$

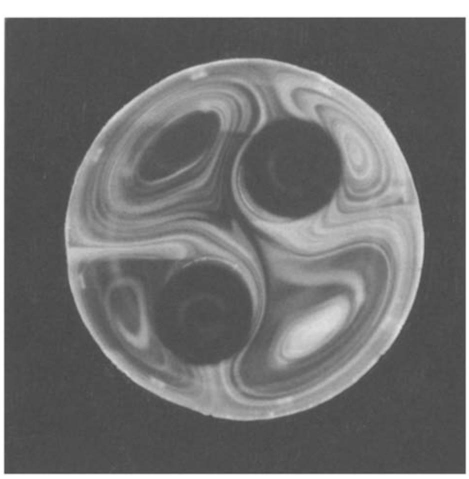

Figure 3 Photograph of flow pattern for Ra = 14,635; $\phi_g = 60°$ and $s/d = 0.8333$

indicated by the comparison of the stream-function extreme shown in Figures 4 and 5. Moreover, the thermal boundary layers on the hot and cold cylinders are seen to become noticeably thinner with the decrease of s/d, resulting in an enhanced heat transfer rate at the cylinders.

In Figure 6, the predicted isotherm distributions for $Ra = 2.93 \times 10^4$, $s/d = 0.8333$ and $\phi_g = 60°$ at $Bi = 0$ and 1.0 are displayed to compare with the corresponding holographic interferogram obtained utilizing a test cell wrapped with an outer insulation blanket of 5cm—the same as constructed in the earlier study (Ho et al. 1993). The holographic interferometry experiment was performed using the adjustment of initial infinite fringe field such that the interference fringes recorded were equivalent to the isotherms of air confined in the enclosure. As revealed in Figure 6, the predicted isotherm distribution with $Bi = 1.0$, in contrast to that for $Bi = 0$, compares favorably with the interferogram, further attesting to the influence of the imperfect thermal insulation encountered in the experiment.

Next, the results of local heat transfer rates on the hot cylinder surface and the circular enclosure wall are presented,

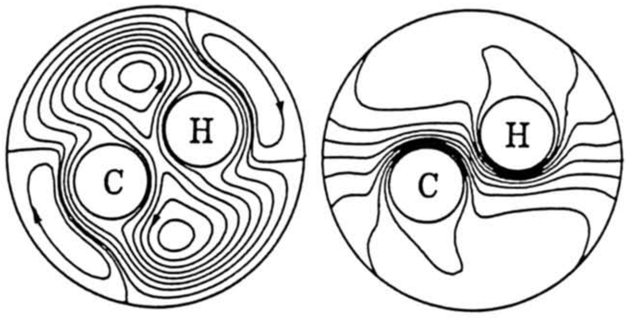

$Ra = 14635 (\psi_{min} = -1.7441, \psi_{max} = 8.7365, \psi_{inner} = 3.5899)$

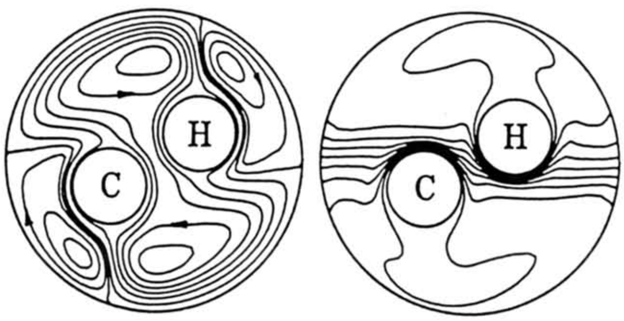

$Ra = 10^5 (\psi_{min} = -6.6608, \psi_{max} = 15.7273, \psi_{inner} = 4.3880)$

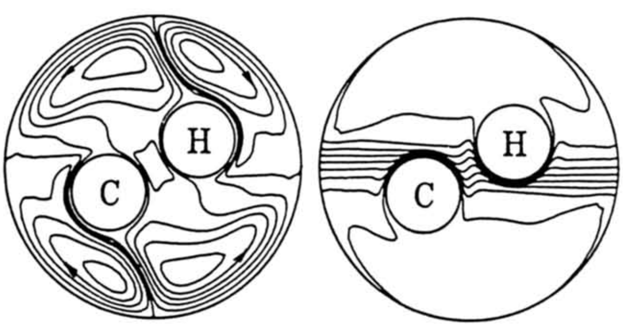

$Ra = 10^6 (\psi_{min} = -21.5097, \psi_{max} = 30.7844, \psi_{inner} = 6.5161)$

Figure 4 Flow patterns and temperature distributions for various Ra with $Bi = 0.5$, $\phi_g = 30°$ and $s/d = 0.7$

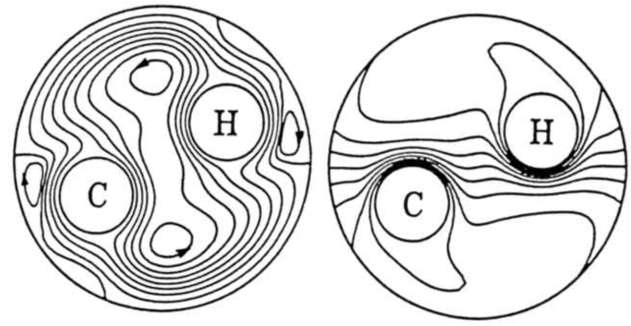

$Ra = 14635 (\psi_{min} = -0.5815, \psi_{max} = 8.3349, \psi_{inner} = 3.1952)$

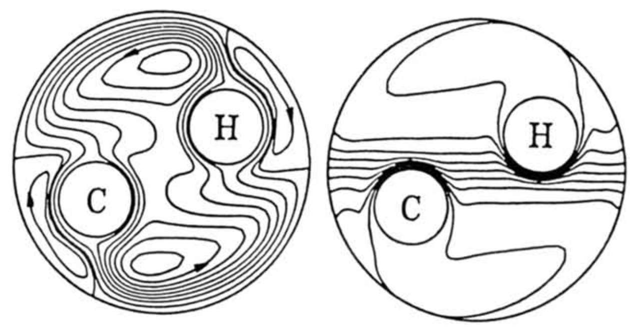

$Ra = 10^5 (\psi_{min} = -2.6252, \psi_{max} = 14.2440, \psi_{inner} = 4.0615)$

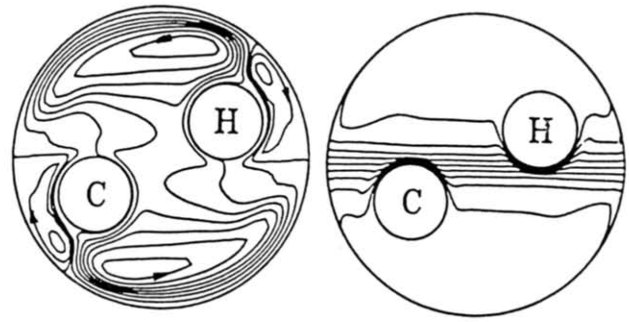

$Ra = 10^6 (\psi_{min} = -7.5317, \psi_{max} = 27.7330, \psi_{inner} = 5.6588)$

Figure 5 Flow patterns and temperature distributions for various Ra with $Bi = 0.5$, $\phi_g = 30°$ and $s/d = 1.0$

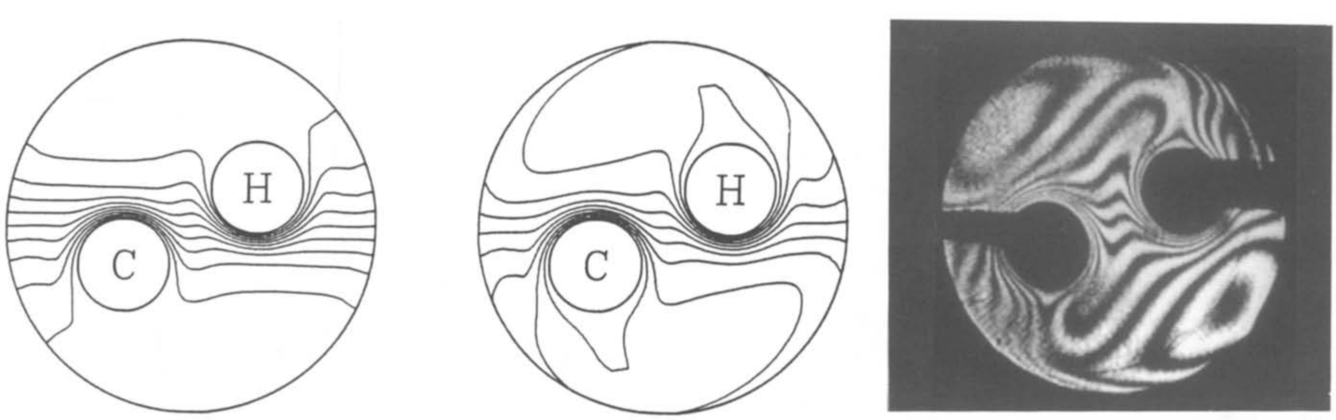

Bi = 0 **Bi = 1.0**

Figure 6 Comparison of isotherm distribution between the prediction and the interferogram for $Ra = 2.93 \times 10^4$, $\phi_g = 30°$ and $s/d = 0.8333$

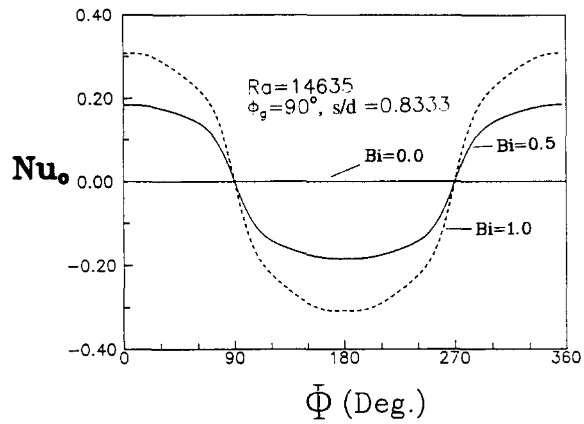

Figure 7 Variations of the local Nusselt number along the enclosure wall at different Bi for $\phi_g = 90°$, $s/d = 0.8333$ and Ra = 14,635

respectively, by means of local Nusselt numbers defined as

$$\mathrm{Nu}_h = \frac{h_h d}{k} = -\frac{\partial \theta}{\partial n} \tag{10a}$$

and

$$\mathrm{Nu}_o = -\frac{\partial \theta}{\partial n} = Bi\theta_o \tag{10b}$$

Here n denotes a normal coordinate to the surface of the hot cylinder or the circular enclosure wall. Further note that a positive value of Nu_o (defined in Equation 10b) indicates a heat flow from air inside the enclosure into the ambient.

Figure 7 conveys the angular profile of the local Nusselt number along the surface of the circular enclosure for three values of Bi at fixed ϕ_g, s/d and Ra. The angular coordinate, Φ, denoted in the abscissa of the figure is measured clockwise from the top of the enclosure wall. As displayed in the figure for the vertical orientation, in the presence of the external heat exchange with the ambient ($Bi \neq 0$), the local heat flux distribution (or equivalently, the surface temperature profile at the enclosure) exhibits a sinusoidal rise/drop-off variation and has a symmetry with respect to the vertical axis of the enclosure. The local heat outflow (positive Nu_o) occurring on the upper half of the enclosure wall decreases angularly from the top until the lower half of the surface is reached, at which the heat inflow from the ambient takes place. Moreover, the sinusoidal variation of the local Nusselt number at the enclosure surface becomes more distinctive as the Biot number is increased. For the inclined orientation $\phi_g = 30°$ and $60°$ (not shown here), the distributions of the local Nusselt number Nu_o, as anticipated, exhibit a slight asymmetry with respect to the vertical axis of the enclosure. This is due to the recirculating flow structure developed inside the enclosure as shown in Figure 2. Furthermore, the increase of Ra, as demonstrated in Figure 8, exerts an effect similar to that of increasing Bi; the sinusoidal rise/drop-off profile of Nu_o becomes more pronounced with the increasing Ra at fixed Bi, ϕ_g and s/d. Another important result worthy of mention is that regardless of the orientation of the enclosure, the circumferentially averaged values of Nu_o for all the simulations undertaken are found to be zero. This means that there is virtually no net heat exchange with the ambient through the enclosure wall, which can be rationalized by the fact that the ambient fluid outside the enclosure for the problem considered here is assumed to be at a mean temperature of the hot and cold cylinder. Accordingly, a steady-state heat transfer balance exists between the differentially heated cylinders within the enclosure, even in the presence of external convection through the enclosure wall.

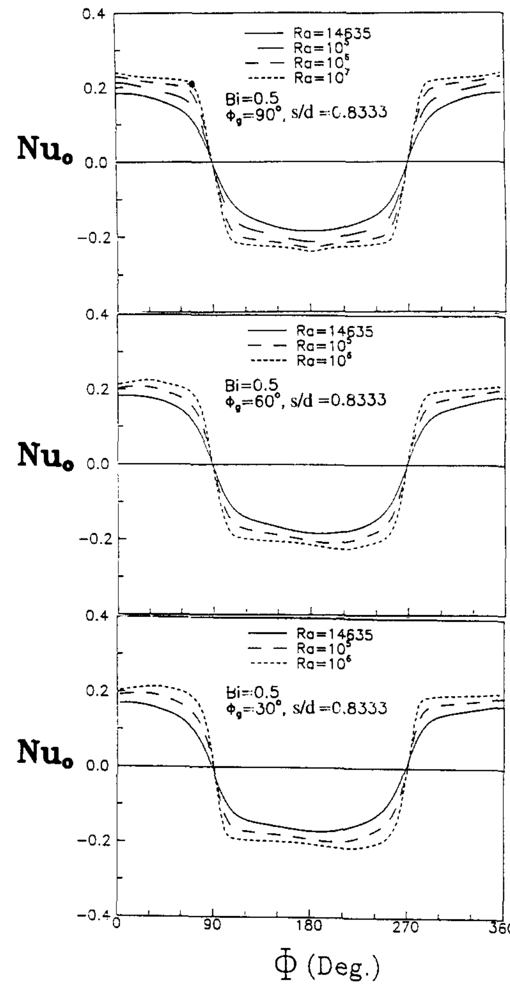

Figure 8 Variations of Nu_o at a different Rayleigh number and orientation angle with $s/d = 0.8333$ and $Bi = 0.5$

In Figure 9, the local Nusselt number at the hot cylinder is plotted against the local angular coordinate Φ for different Bi and ϕ_g, with $s/d = 0.8333$ and Ra = 14,635. An overview of the figure reveals that the heat transfer at the hot cylinder mainly takes place on the lower half of the surface. Furthermore, the effect of Bi on the local heat transfer profile appears to be a function of the orientation angle ϕ_g. For the vertical orientation $\phi_g = 90°$, the increase of Bi leads to a substantially higher heat transfer rate at the hot cylinder, but this enhancing effect tends to degrade with the smaller orientation angle. At $\phi_g = 30°$, as shown in Figure 9, the enhanced external convection associated with the increase of Bi causes the local Nusselt number distribution at the hot cylinder to become somewhat less localized.

Finally, the circumferentially averaged Nusselt number on the hot cylinder is plotted as a function of the Rayleigh number for different values of Bi, s/d and ϕ_g, as displayed in Figure 10. The average heat transfer rate from the hot cylinder is clearly a function of Ra, Bi, s/d and ϕ_g. As generally expected, the overall heat transfer rate increases with the increase of Ra. In the presence of external convection, the effects of the inclination angle of the enclosure and the gap width between cylinders on the average Nusselt number $\overline{\mathrm{Nu}}_h$ appear to be similar to those found for the adiabatic enclosure (Ho et al. 1993). The increase of ϕ_g or s/d can give rise to a substantial decrease of the average

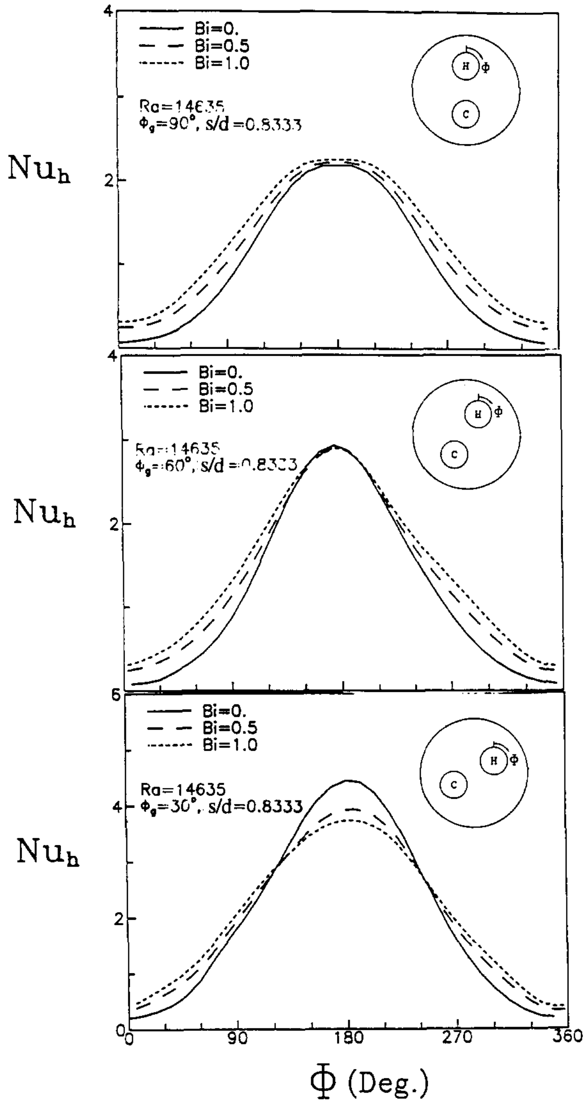

Figure 9 Effect of *Bi* on the local heat transfer rate of the hot cylinder at a different orientation with $s/d = 0.8333$ and Ra = 14,635

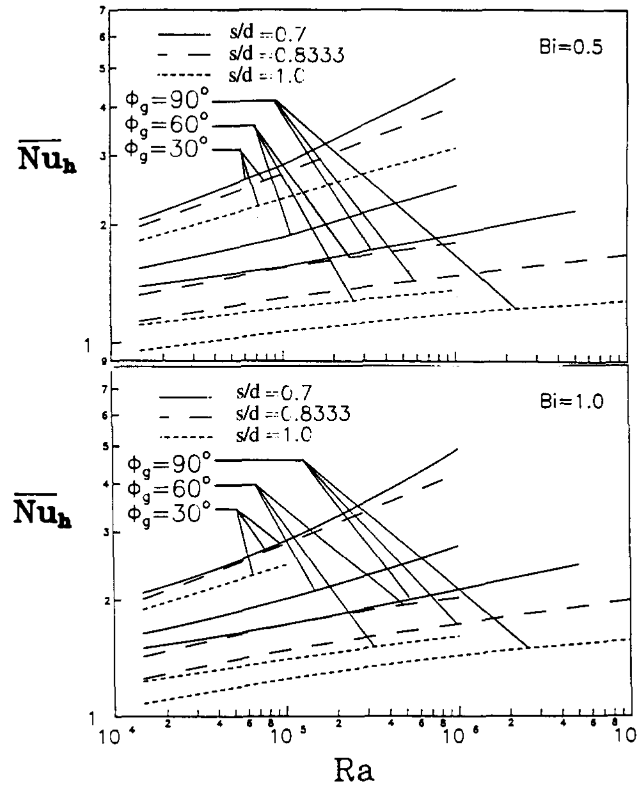

Figure 10 Relation of the average Nusselt number at the hot cylinder with the Rayleigh number

heat transfer rate from the hot cylinder. Moreover, by means of a least squares regression analysis, the average Nusselt number of the hot cylinder for different *Bi*, *s/d* and ϕ_g can be correlated versus the Rayleigh number in the form of

$$\overline{\mathrm{Nu}}_h = C\,\mathrm{Ra}^m \tag{11}$$

where the coefficients *C* and *m* are listed in Table 1. The effects of the geometric parameters on the buoyant-convection heat transfer at the hot cylinder are further shown by the decreasing values of the exponent *m* with the increase of either ϕ_g or *s/d* as shown in the table. The average deviations listed in Table

Table 1 Constants *C* and *m* for Equation 11

Bi	*s/d*	ϕ_g(°)	Ra	*C*	*m*	Average deviation (percent)
0.5	0.7	30	10^4–10^6	0.3066	0.1964	2.55
		60	10^4–10^6	0.4993	0.1171	1.71
		90	10^4–5×10^6	0.6491	0.0778	1.30
	0.8333	30	10^4–10^6	0.3889	0.1690	0.80
		60	10^4–10^6	0.6629	0.0728	0.88
		90	10^4–10^7	0.6460	0.0598	0.84
	1.0	30	10^4–10^6	0.5289	0.1288	0.07
		60	10^4–10^6	0.7011	0.0483	0.26
		90	10^4–10^7	0.6283	0.0452	1.36
1.0	0.7	30	10^4–10^6	0.2918	0.2021	3.58
		60	10^3–10^6	0.4974	0.1231	1.3
		90	10^4–10^7	0.6551	0.0854	0.9
	0.8333	30	10^4–10^6	0.3713	0.1757	0.56
		60	10^4–10^6	0.6532	0.0825	1.34
		90	10^4–10^7	0.6402	0.0714	1.27
	1.0	60	10^4–10^6	0.6729	0.0632	0.31
		90	10^4–10^7	0.6337	0.0575	1.82

1 are the standard error of the estimate around the regression line in terms of the fractional relative discrepancy between the values evaluated using Equation 11 and the corresponding numerical data (Chapra and Canale 1988).

Concluding remarks

In the present study, numerical simulations via a finite-difference method have been carried out for the problem of buoyancy-driven fluid flow and heat transfer of air between two horizontal, differentially heated circular cylinders confined to a circular enclosure subjected to external convection. Numerical results demonstrate that the presence of heat exchange of air inside the enclosure with the ambient, at the mean temperature of the hot and cold cylinder, may lead to greatly intensified buoyant flow and temperature fields inside the enclosure. Thus, a substantially enhanced heat exchange arises between the two cylinders. For all the simulations undertaken, there is virtually no net heat exchange of air inside the enclosure with the ambient. This implies that for energy-efficient operation of a heat-tracing system, it is better to set the hot cylinder (tracer) temperature so that the mean temperature of the hot and cold cylinder (pipe) is close as possible to the ambient. Moreover, the effects of varying the Rayleigh number, the orientation angle of the enclosure and the gap width between the two cylinders in the presence of external convection are found to be similar to those observed in an adiabatic enclosure. In addition, the simulation taking into account the external heat exchange at the enclosure wall appears to compare favorably with the experimental observation of flow structure and temperature distribution inside a test cell that could not be perfectly insulated thermally.

Acknowledgments

The authors gratefully acknowledge the support for the present study from the National Science Council of the Republic of China through project NSC 81–0401–E006–03. The constructive comments of the reviewers leading to improvement of the earlier manuscript are sincerely appreciated.

References

Adlam, J. H. 1986. Computation of two-dimensional time-dependent natural convection in a cavity where there are internal bodies. *Computers & Fluids*, **14**(2), 141–157

Chapra, S. C. and Canale, R. P. 1988. *Numerical Methods for Engineers*. McGraw-Hill, Inc., New York

Crupper, G. and Warrington, R. O. 1981. Natural convection heat transfer between tube bundles and a cubical enclosure. *Journal of Heat Transfer*, **103**(1), 103–107

Ho, C. J. and Lin, Y. H. 1991. Natural convection in a horizontal annulus partially filled with cold water. *Int. J. Heat Mass Transfer*, **34**(6), 1371–1382

Ho, C. J., Chang, W. S. and Wang, C. C. 1993. Natural convection between two horizontal cylinders in an adiabatic circular enclosure. *Journal of Heat Transfer*, **115**, 158–165

Kline, S. J. and McClintock, F. A. 1953. Describing uncertainty in single-sample experiments. *Mechanical Enginering*, **January**, 3–12

Kohli, I. P. 1979. Steam tracing of pipelines. *Chemical Engineering*, **March**, 156–163

Lacroix, M. 1992. Natural convection heat transfer around two horizontal cylinders inside a rectangular cavity cooled from above. *Numerical Heat Transfer, Part A*, **21**, 37–54

Sandberg, C. 1989. Heat tracing: steam or electric? *Hydrocarbon Processing*, **March**, 107–110

Thomas, P. D. and Middlecoff, J. F. 1980. Direct control of the grid point distribution in meshes generated by elliptic equations. *AIAA Journal*, **18**, 562–656

Thompson, J. F., Thames, F. C. and Mastin, C. F. 1974. Automatic numerical generation of body-fitted curvilinear coordinate system for fluid containing any number of arbitrary two-dimensional bodies. *Journal of Computational Physics*, **15**, 299–319

Warrington, R. O. and Weaver, R. A. 1990. Natural convection heat transfer between arrays of horizontal cylinders and their enclosure. *Heat Transfer–1990*, **2**, 205–209